PAPER NUMBER

26

CORROSION 90

April 23-27, 1990 · Bally's Hotel, Las Vegas, Nevada

# EROSION-CORROSION UNDER DISTURBED FLOW CONDITIONS IN SLURRY PIPELINES

S. Nesic and J.Postlethwaite
Department of Chemical Engineering
University of Saskatchewan
Saskatoon, SK
Canada, S7N 0W0

## ABSTRACT

Flow dependent erosion-corrosion often occurs under disturbed flow conditions at geometrical irregularities such as fittings, valves and weld beads. Flow separation and reattachment produces high turbulence intensity and particle–wall interactions that can lead to high erosion–corrosion rates.

This paper presents the predictions of 2-D turbulent, single and two-phase liquid/particle flow with recirculation, after a sudden constriction and expansion. The model is based on a two-phase flow version of a standard $k-\epsilon$ model of turbulence and a stochastic simulation of particle-fluid turbulence interactions. It is capable of successfully predicting local values of time averaged fluid velocities and turbulence intensities, as well as predicting particle dispersion, and particle–wall interaction.

The numerical predictions of the flow structure are used to explain the results of an experimental erosion–corrosion study of a slurry flowing in a pipe with a sudden constriction and expansion. It is shown that in case of disturbed flow it is appropriate to correlate local near–wall parameters of flow with the metal loss rates. The simulations have shown that local near–wall intensity of turbulence is the important factor affecting mass transfer controlled corrosion in disturbed flow, rather than the wall shear stress. In case of pure corrosion, comparisons revealed a significant effect of local turbulence intensity on corrosion rate of the base metal. In case of erosion–corrosion, maximum metal loss coincided with local maximums of particle–wall mean impact frequency.

Key words: erosion–corrosion, flow dependent corrosion, slurry flow, $k-\epsilon$ model of turbulence.

## INTRODUCTION

Oxygen–mass transfer controlled erosion–corrosion in straight slurry pipelines can be modelled by the application of appropriate mass transfer correlations which relate the Sherwood, Schmidt and Reynolds numbers [1,2]. This simple approach cannot be applied to erosion–corrosion in many practical situations [3], where the metal loss occurs under conditions of disturbed flow at geometrical irregularities [4], such as weld beads and fittings, where the flow separates and/or impinges on the walls. A knowledge of the local flow structure and related turbulence intensity along with details of particle wall interactions is required in order to model such erosion–corrosion. The objectives of modelling are to elucidate the mechanism of the metal loss, distinguishing between pure erosion and mass transfer controlled erosion–corrosion. The ultimate goal is to develop a successful predictive model which would contribute to better design of slurry flow systems.

This paper describes the development of a model for determining structure of the flow in dilute slurries and its application to the results of a recent experimental study [5] of erosion–corrosion at a constriction and a expansion in a pipe.

## EXPERIMENTAL WORK

An experimental investigation on the effect of wall geometry and resulting flow structure on erosion–corrosion was conducted [5] in a tubular test cell (Fig.1). The form of the cell enabled two different geometries to be studied at the same time: a sudden constriction and a sudden expansion. The test cell was segmented in order to enable measurements of local weight loss.

The segmented test cell material was carbon steel (AISI MT - 1015). The test medium was 3 wt% *NaCl* (technical grade in distilled water) with and without 2 vol% silica sand. The test conditions are listed in Table 1.

## LIQUID/PARTICLE FLOW MODEL

The turbulent fluid flow field was modelled by a well established Eulerian based, control volume procedure, for solution of time averaged flow equations. The motion of a dispersed particulate phase can be determined by both Lagrangian or Eulerian methods, depending on whether particles are treated as a "second fluid" [6], or a large number of representative trajectories are calculated in the flow domain [7]. According to a numerical study [8] both methods have their advantages, but for the case of particle size distributions and significant particle–wall interactions, the Lagrangian approach seems advantageous, since it gives more information about the particles.

### Assumptions

The following assumptions were made:

- Particles are treated as sources or sinks of momentum, mass and energy in the fluid;
- Particles have a negligibly small volume compared to the total volume of the flow;
- Direct particle-particle interactions are negligible, but fluid-particle interactions lead to a two-way coupling;
- External fluxes and stresses act directly on the fluid only;
- Brownian movement of the particles or movement due to pressure gradients and particle rotation is neglected;
- Particles are spherical.

### Fluid-Phase Flow Equations

The present model is based on a standard single phase $k-\epsilon$ model of turbulence proposed by Launder and Spalding [9]. The conservation equations for mass, momentum, kinetic energy of turbulence and it's dissipation are presented for the case of two-dimensional, axis-symmetrical flow – Appendix A.

All conservation equations for the fluid phase can be written in a general form:

$$\underbrace{\frac{\partial}{\partial x_i}(\rho U_i \Phi)}_{convection} = \underbrace{\frac{\partial}{\partial x_i}(\Gamma_\Phi \frac{\partial \Phi}{\partial x_j})}_{diffusion} + \underbrace{S_\Phi}_{source} \tag{1}$$

or for turbulent, axisymmetrical liquid/particle flow:

$$\frac{\partial}{\partial x}(\rho U \Phi) + \frac{1}{r}\frac{\partial}{\partial r}(r\rho V \Phi) = \frac{\partial}{\partial x}(\frac{\mu_{eff}}{\sigma_\Phi}\frac{\partial \Phi}{\partial x}) + \frac{1}{r}\frac{\partial}{\partial r}(r\frac{\mu_{eff}}{\sigma_\Phi}\frac{\partial \Phi}{\partial r}) + S_\Phi + S_\Phi^p \tag{2}$$

where $\Phi = U, V, W, k, \epsilon, \ldots$

This enables application of an universal solution procedure, based on the SIMPLE algorithm by Patankar and Spalding [10], for all equations. This algorithm includes discretization of the partial differential equations by using a control volume method, which gives a clear physical picture of the flow.

In case of a two-phase liquid/particle flow the solution procedure has the following steps:

1. solution of the fluid (single-phase) flow equations until a reasonably converged solution is obtained;
2. calculation of the particle trajectories and particle source terms for the fluid flow equations;
3. solution of the fluid flow equations with new source terms;
4. check for convergence, if not reached go to step 2;
5. final calculations and printout.

Mean particle flow properties and the phase interaction source terms $S_\Phi^p$ in the fluid flow equations (2), are calculated directly in the part of the program for particles by averaging a large number of particle trajectories.

### Motion of Particles

The motion of particles in fluid turbulence is predicted by means of Lagrangian Stochastic-Deterministic model (LSD), proposed by Milojevic [7]. The numerical solution of fluid flow equations provides the fields of mean fluid velocity components and kinetic energy of turbulence $k$ and dissipation $\epsilon$. From algebraic relations for normal turbulent stresses all three components of the fluctuation velocity can be determined. Knowing local $k$ and $\epsilon$ values, it is possible to estimate turbulence time and length scales, corresponding to the large, energy containing eddies. Particle trajectories from the inlet to the outlet of the flow domain are then calculated by numerical solution of "instantaneous" particle momentum equation (17) – Appendix B.

## RESULTS AND DISCUSSION

Before any predictions are shown it is important to point out that the hydrodynamic tests of a similar numerical model to the one used in this work were done by Milojevic [7]. He compared his predictions with three different experiments from literature by: Snyder and Lumley [11], Wells and Stock [12] and Arnason [13], and obtained a good agreement for the dispersion of particles in a turbulent air flow field, for all three test cases. Milojevic [7] also compared his predictions with his own results of local flow measurements using Laser–Doppler anemometry in a two-dimensional confined two-phase jet flow. His results were good although some discrepancies were found in the region close to the wall due to the wall-function approach for modelling the boundary layer flow.

### Prediction Procedure

In order to cover the flow field, a computational grid 93 x 26 nodes was set up. Such a large number of computational points was a consequence of the long and narrow shape of the flow region ($700 \times 40mm$) and constraints related to suggested (reasonably small) control volume aspect ratio (1:10) and expansion factor (1.25).

The criteria for convergence was the cumulative error over all the control volumes and was set to 0.1%. In the case of pure water flow the final solution was reached in about 700 iterations. In case of a 2% slurry flow, 90 different starting locations and 2000 different trajectories were calculated in every call of the program for particle motion. In this case about 1100 iterations were needed to reach the converged solution.

Since no fluid flow measurements were available, a fully developed turbulent flow velocity profile was assumed 12 diameters before the constriction. For the particles a terminal velocity on the inlet was given. No particle turbulence was assumed at the inlet although numerical tests have shown that this condition, in our case, does not influence the results. A unique particle size of 430 $\mu$m was used for predictions, thus neglecting the narrow particle size distribution present in the experiments.

### Comparison of Simulation and Experimental Results

Fluid flow results. Some of the most important features obtained by the simulations are given in Figures 2–4. Fig.2a and 3a show streamlines, representing the mean flow in case of pure water flow (Fig.2a) and 2% slurry flow (Fig.3a). The streamlines show: (a) strong curvature of the flow in front of the constriction and associated with it a small recirculation eddy in the corner and (b) separation of the main flow stream at the expansion edge and reattachment further downstream resulting in a large recirculation zone in the corners.

Figures 2b and 3b show the predicted field of turbulent fluctuations. Fluctuations are assumed isotropic and are calculated from the field of kinetic energy of turbulence. It is noticeable that the flow geometry generates two main sources of turbulence: one close to the constriction corner and a much larger one after the expansion. They are both a function of large mean velocity gradients that exist at these points, causing significant shear stress and turbulence. In the case of slurry flow the pattern of turbulent fluctuations (Fig.3b) is similar to the one for water flow (Fig.2b), except that the particles distort the turbulence field by accepting some of the turbulence energy at peak points and redistributing it further downstream. This effect is not big due to the small particle volume concentration (2%).

Flow dependent corrosion. As we are primarily interested in the effect that the flow structure has on corrosion it is important to determine the mean flow parameters close to the walls, that are affecting the rate of oxygen-mass transfer controlled corrosion.

In a review Syrett [14] has indicated that a critical value for *velocity* ("breakaway velocity") has been used as a useful criterion for determining initiation of accelerated corrosion. Some other authors experimenting with flow dependent corrosion in straight pipes [15] and rotating cylinders [16], have suggested that *shear stress* is the more appropriate parameter of flow that can be directly related to local rate of mass transfer and corrosion. They have also determined values for "critical shear stress" for different materials and liquids. The term *turbulence intensity* has been used interchangeably with shear stress relating it to rates of corrosion. Blatt et al.[17] have reported experimental evidence that local maxima in corrosion in disturbed flow conditions coincide with maximum values of local turbulent fluctuations. They have used a Laser-Doppler Anemometry for fluid flow measurements and both electrochemical

and weight loss techniques for for corrosion measurements.

It is quite clear,from literature, that in case of disturbed flow the mean velocity or a Reynolds number cannot be used as effective criteria to correlate mass transfer rates. However for shear stress this is not as obvious. Fig.4 shows predicted variation of wall shear stress (4a) along with the pattern of corrosion along the main pipe wall (4b). Predicted average levels of wall shear stress $50-300Pa$ are, according to [15], within the range of critical shear stresses needed for removal of protective films for copper based alloys in sea water. The pattern of wall shear stress is similar to the pattern of corrosion, except for the region after the expansion. According to the wall shear stress pattern, there should be a minimum of the corrosion rate somewhere close to the reattachment point ($x \approx 0.37m$, where the shear stress is zero), but the measured rate of metal loss indicates actually the opposite: there is a local maximum in this region. This suggested that there is some other factor governing the enhanced rate of mass transfer controlled corrosion.

Fig.2c shows predicted close to wall turbulent intensity expressed in terms of turbulent fluctuations. When compared to the rates of metal loss measured in the segmented cell specimen (Fig.2d) the overall similarities in profile shape are obvious, including the region after the expansion. This suggested that **close to wall turbulence intensity can be used as an effective criterion to be correlated with rates of mass transfer**, which is in agreement with the recent experimental findings of Blatt et al.[17].

It is now relatively straightforward to explain why in cases of straight pipe flow or rotating cylinders values of shear stress correlate the mass transfer rates. In those simple flow geometries the patterns of wall shear stress were the same as patterns of near–wall turbulence intensity, because wall friction was the main generator of turbulence. The same argument can be used for the straight parts of the pipe in the presented experimental results. But when there is separation and reattachment of flow, there are other sources of turbulence such as: large gradients in the mean axial velocity in the fluid bulk after the expansion (Fig.2b). In these cases the near–wall profiles of turbulence intensity and shear stress do not have to correspond. Formed turbulent eddies are transported by convection from the regions where they form and if they reach the walls they alter the near–wall turbulent intensity profile. Thus a local maximum of turbulence intensity close to the wall after the expansion (Fig.2c, $x \approx 0.33m$) is a reflection of the overall maximum of turbulence intensity in the bulk close by (Fig.2b).

Fig.2c shows the predicted peak of turbulence intensity close to the constriction edge which was not recorded in the experiments as a peak in metal loss, but low resolution and accuracy of measurements in this region prevents us from drawing any further conclusions. A much shorter specimen should be used at the leading edge of the constriction in future experiments.

The question to be answered now is: how does turbulence enhance local rates of mass transfer? As a first approximation we can assume that rate of mass transfer is controlled by the resistance in the protective corrosion film on the metal surface and the resistance in the boundary layer. Shemilt et al. [18] have found that the mass transfer coefficient in the boundary layer ("damped turbulence layer") controls the overall mass transfer rate. Lotz and Postlethwaite [5] in their experimental study have found the opposite: that the coefficient for mass transfer in the protective corrosion layer is much higher than the one for the boundary layer. Hence intensive turbulence close to the wall probably affects both: disturbs the mass transfer boundary layer, and thins the protective corrosion layer, but to what extent one of these two mechanisms is governing the overall mass transfer rate, seems unclear at this point and needs further research.

Fig.2d shows the amount of scale retained in the experiments, (as the shaded area), suggesting that actually the protective corrosion products were only partially removed from the metal surface by intensive turbulent fluctuations near the wall, to enable higher oxygen transfer rates to the surface and higher levels of corrosion. The scale retention ratio **R** is defined as:

$$\mathbf{R} = \frac{local\ mass\ of\ scale}{local\ metal\ mass\ loss} \tag{3}$$

Flow dependent erosion-corrosion. For 2% slurry flow the profile of near–wall turbulence intensity (Fig.3c) differs very little from the one for water flow (Fig.2c). Again, it has a similar character as the erosion–corrosion profile recorded in the experiments with 2% slurry flow (Fig.3d). But it is important to notice that the whole

erosion–corrosion profile for slurry flow (Fig.3d) has been elevated compared to the corrosion profile for water flow (Fig.2d), while the predicted turbulence profile remained nearly unchanged. This suggests that particles have some other effect on accelerating metal loss other than altering the turbulence field. The high rate of metal loss at the front facing constriction wall and the very small amount of scale retained (Fig.3d), suggest that **particle wall impacts (erosion) are that important factor which causes further thinning of the protective layer on the surface** and even erosion of the base metal itself. Thus predicted particle–wall impact *statistics* (mean local values of impact frequency, velocity and angle, obtained from averaging over the large number of particle trajectories), were analyzed in an attempt to explain noticed differences. The predictions have indicated significant particle–wall impact rates only in the regions of strong curvature of the flow: at the constriction and after the expansion. Predicted frequency of particle–wall impacts at the front facing constriction wall was about 200 $/(mm^2 s)$ while downstream of the constriction it was an order of magnitude lower (5-20 $/(mm^2 s)$) The average particle impact velocities perpendicular to the wall were in the range of $v^p = 0.2 - 1.1 m/s$ while the the average angles of impact varied from $10 - 80$ degrees on the front facing wall and $0 - 40$ degrees after the expansion. These results explain the large peak in metal loss at the front facing constriction wall and the higher erosion–corrosion rates downstream from the expansion. But the predictions do not suggest a reason for the elevated rate of metal loss along the constricted pipe wall in case of slurry flow. Two explanations are possible: (1) the accuracy of predicted particle–wall statistics is still not high enough or (2) there is some other mode through which particles influence higher erosion–corrosion rate other than altering the turbulence field and direct impact erosion.

## CONCLUSIONS

1. In order to predict rates of corrosion and erosion–corrosion for the case of disturbed single or two-phase flow, it is necessary to determine the local, near–wall structure of the flow and particle–wall impact statistics. Knowledge of overall hydrodynamic and/or geometrical parameters is not sufficient. Thus, simulation of the flow structure is needed.

2. In disturbed flow, wall shear stress is not the governing factor for mass transfer controlled corrosion, but rather it is the local near–wall intensity of turbulence. In case of straight pipe flow the two coincide.

3. In case of pure corrosion (single-phase flow), comparisons revealed a significant effect of local turbulence intensity on corrosion rate of the base metal. It has been hypothesized that intensive near–wall turbulence contributed to disrupting the protective corrosion layer and disturbed the mass transfer boundary layer, thus enhancing oxygen transport and metal loss by corrosion.

4. In case of erosion–corrosion (two-phase flow), maximum metal loss coincided with local maximums of particle–wall mean impact frequency (front facing wall and downstream from the expansion). A similar pattern of metal loss was observed as in case of pure corrosion, but at a higher level. Similarity of the pattern has been attributed partially to the pattern of turbulence that is only slightly different in case of 2% slurry flow compared to water flow. Large rates of metal loss at the front facing wall and overall higher level of erosion–corrosion have been assumed to be the consequence of particle–wall impacts, that is erosion of the protective film.

## NOTATION

$A^p$ - projected area for the particle
$C_\mu, C_D, C_1, C_2, C_3$ - constants in $k - \epsilon$ model of turbulence
$C_D$ - drag coefficient
$d^p$ - particle diameter
$E$ - constant in the logarithmic wall function
$f^p$ - drag coefficient for flow around a sphere
$F$ - force
$k$ - kinetic energy of turbulence
$L_L$ - length scale of turbulence

$L_\epsilon$ - length scale for dissipation
$m^p$ - particle mass
$p$ - pressure
$r$ - radial coordinate
$\mathbf{R}$ - retention ratio
$Re$ - Reynolds number
$s_{i,j}$ - fluctuation component of the rate of strain
$s^p_{u_i}$ - fluctuation component of the particle momentum source term
$S$ - source term
$t$ - time
$T_L$ - Lagrangian integral time scale
$u, v, w$ - components of the fluctuation velocity vector
$U, V, W$ - components of mean velocity vector
$\tilde{u}, \tilde{v}, \tilde{w}$ - components of the instantaneous velocity vector
$u', v', w'$ - means of the components of fluctuation velocity (RMS)
$U^+$ - nondimensional velocity
$U_\tau$ - shear velocity
$V$ - mean radial velocity
$\vec{V}$ - velocity vector
$x$ - axial coordinate
$y^+$ - nondimensional distance from the wall

**Greek letters**
$\Gamma$ - diffusion coefficient
$\delta$ - Kronecker's delta
$\epsilon$ - dissipation of kinetic energy of turbulence
$\Phi$ - general variable
$\Psi_R$ - particle–wall reflection coefficient
$\kappa$ - constant in the logarithmic wall function
$\mu$ - dynamic viscosity
$\rho$ - fluid, density
$\sigma_k, \sigma_\epsilon, \sigma_\Phi$ - turbulent Prandtl-Schmidt numbers
$\tau_w$ - wall tangential shear stress

**Superscripts**
$p$ - refers to particles
$\tilde{}$ - stands for instantaneous value

**Subscripts**
$c$ - refers to point $c$ close to the wall
$eff$ - refers to effective value (molecular + turbulent)
$i, j, l$ - refer to coordinate directions $x, y, z$
$k$ - refers to kinetic energy of turbulence
$t$ - refers to turbulent value
$U, V, W$ - refers to components of mean velocity
$w$ - refers to a wall value
$\epsilon$ - refers to dissipation of kinetic energy of turbulence
$\Phi$ - refers to a general variable

## REFERENCES


1. J.Postlethwaite, Mater. Perf., Vol.26, No.12, p.41, 1987.
2. J.Postlethwaite, M.H.Dobbin, K.Bergevin, Corros., Vol.42, p.514, 1986.
3. B.C.Syrett, S.S.Wing, Corros., Vol.36, p.73, 1980.
4. W.Glaeser, "Erosion–Corrosion Cavitation and Fretting, Forms of Corrosion Recognition and Prevention", ed. C.P.Dillon, Nace, Houston, 1982.
5. U.Lotz, J.Postlethwaite "Erosion–Corrosion in Disturbed Two Phase Liquid/Particle flow", Corros. Sci.,in press, 1989.
6. F.Pourahmadi, J.A.C.Humphrey, Physico–Chemical Hydrodynamics, Vol.4, p.191, 1983.
7. D.Milojevic, T.Borner, F.Durst, "Prediction of Turbulent Gas-Particle Flow Measurement in a Plain Confined Jet", World Congress Particle Technology, Part IV, Partikel Technologie Nurnberg, Nurnberg, W.Germany, 1986.
8. T.Durst,D.Milojevic,B.Schonung, Appl. Math. Model., Vol.8, p.101, 1984.
9. B.E.Launder, D.B.Spalding, Computer Methods in Applied Mechanics and Engineering, Vol.3, p.269, 1974.
10. S.V.Patankar, D.B.Spalding, Int. J. Heat Mass Transfer, Vol.16, p.1119, 1973.
11. W.H.Snyder, J.L.Lumley, J. Fluid Mech., Vol.48, p.41, 1971.
12. D.E.Stock J. Fluid Mech., Vol.136, p.31, 1983.
13. G.Arnason, "Measurement of Particle Dispersion in Turbulent Pipe Flow" Ph.D. thesis, Washington State University, Pullman, 1982.
14. B.C.Syrett, Corros., Vol.32, p.242, 1976.
15. K.D.Efird, Corros., Vol.33, p.3, 1977.
16. D.C.Silverman, Corros., Vol.40, p.220, 1984.
17. W.Blatt, T.Kohley, U.Lotz, E.Heitz, "The Influence of Hydrodynamics on Erosion–Corrosion in Two-Phase Liquid/Particle Flow", to appear in Corros..
18. L.W.Schemilt, C.Y.Cha, E.Fiadzigbe, A.B.Ponter, Corros. Sci., Vol.20, p.443, 1980.

## APPENDIX A

### Fluid Flow Equations

Reynolds decomposition for fluctuating variables and time averaging of instantaneous fluid flow equations yields:

*Continuity equation:*

$$\frac{\partial}{\partial x}(\rho U) + \frac{1}{r}\frac{\partial}{\partial r}(r\rho V) = 0 \tag{4}$$

*Momentum equation in axial direction:*

$$\frac{\partial}{\partial x}(\rho U^2) + \frac{1}{r}\frac{\partial}{\partial r}(r\rho UV) = \frac{\partial}{\partial x}(\mu_{eff}\frac{\partial U}{\partial x}) + \frac{1}{r}\frac{\partial}{\partial r}(r\mu_{eff}\frac{\partial U}{\partial r}) + \frac{\partial}{\partial x}(\mu_{eff}\frac{\partial U}{\partial x}) + \frac{1}{r}\frac{\partial}{\partial r}(r\mu_{eff}\frac{\partial V}{\partial x}) - \frac{\partial p}{\partial x} + S_U^p \tag{5}$$

*Momentum equation in radial direction:*

$$\frac{\partial}{\partial x}(\rho UV) + \frac{1}{r}\frac{\partial}{\partial r}(r\rho V^2) = \frac{\partial}{\partial x}(\mu_{eff}\frac{\partial V}{\partial x}) + \frac{1}{r}\frac{\partial}{\partial r}(r\mu_{eff}\frac{\partial V}{\partial r}) + \frac{\partial}{\partial x}(\mu_{eff}\frac{\partial U}{\partial r}) + \frac{1}{r}\frac{\partial}{\partial r}(r\mu_{eff}\frac{\partial V}{\partial r}) - 2\mu_{eff}\frac{V}{r^2} - \frac{\partial p}{\partial r} + S_V^p \tag{6}$$

In equations (5) and (6) Boussinesq assumption has been used for modelling the Reynolds stress. In case of isotropic turbulence it is:

$$-\rho\overline{u_i u_j} = \mu_t(\frac{\partial U_i}{\partial x_j} + \frac{\partial U_j}{\partial x_i}) - \frac{2}{3}\rho k\delta_{ij} \tag{7}$$

where $\mu_t$ is "turbulent viscosity":

$$\mu_t = C_\mu\frac{\rho k^2}{\epsilon} \tag{8}$$

Kinetic energy of turbulence $k$ and it's dissipation $\epsilon$ are:

$$k = \frac{1}{2}\overline{u_i u_i}, \qquad \epsilon = 2\frac{\mu}{\rho}\overline{s_{ij}s_{ij}} \tag{9}$$

*Equation for kinetic energy of turbulence:*

$$\frac{\partial}{\partial x}(\rho U k) + \frac{1}{r}\frac{\partial}{\partial r}(r\rho V k) = \frac{\partial}{\partial x}(\frac{\mu_{eff}}{\sigma_k}\frac{\partial k}{\partial x}) + \frac{1}{r}\frac{\partial}{\partial r}(r\frac{\mu_{eff}}{\sigma_k}\frac{\partial k}{\partial r}) + G_{k1} - \rho\epsilon + S_k^p \tag{10}$$

*Equation for dissipation of kinetic energy of turbulence:*

$$\frac{\partial}{\partial x}(\rho U \epsilon) + \frac{1}{r}\frac{\partial}{\partial r}(r\rho V \epsilon) = \frac{\partial}{\partial x}(\frac{\mu_{eff}}{\sigma_\epsilon}\frac{\partial \epsilon}{\partial x}) + \frac{1}{r}\frac{\partial}{\partial r}(r\frac{\mu_{eff}}{\sigma_\epsilon}\frac{\partial \epsilon}{\partial r}) + \frac{\epsilon}{k}(C_1 G_{k1} - C_2\rho\epsilon) + S_\epsilon^p \tag{11}$$

In equations (10) and (11) generation of kinetic energy of turbulence $G_{k1}$ is:

$$G_{k1} = \mu_{eff}\{2[(\frac{\partial U}{\partial x})^2 + (\frac{\partial V}{\partial r})^2 + (\frac{V}{r})^2] + (\frac{\partial U}{\partial r} + \frac{\partial V}{\partial x})^2\} \tag{12}$$

Effective viscosity $\mu_{eff}$ is:

$$\underbrace{\mu_{eff}}_{effective} = \underbrace{\mu}_{molecular} + \underbrace{\mu_t}_{turbulent} \tag{13}$$

Used constants are the same as for single–phase flow:

$$C_\mu = 0.09, \qquad C_1 = 1.44,$$
$$C_2 = 1.92, \qquad C_3 = 0.7,$$
$$\sigma_k = 1.0, \qquad \sigma_\epsilon = 1.3$$

In equations (5) and (6) $S_U^p$ and $S_V^p$ are the sources or sinks of momentum due to the presence of particles and are equal to the summary drag force for all the particles in the control volume. They can be calculated directly, in the course of the simulation of the particle motion. The sources or sinks of kinetic energy of turbulence $S_k^p$ and dissipation $S_\epsilon^p$ in equations (10) and (11) are:

$$S_k^p = \overline{s_{u_i}^p u_i} \tag{14}$$

$$S_\epsilon^p = \mu\overline{\frac{\partial s_{u_i}^p}{\partial x_l}\frac{\partial ui}{\partial x_l}} \tag{15}$$

and can also be directly calculated from a large number of particle trajectories.

Equations for the fluid phase are very similar in the Cartesian $x - y$ coordinate system and can be readily derived from above, by setting:

$$\frac{\partial}{\partial r} = \frac{\partial}{\partial y}, \qquad r = 1, \qquad \frac{1}{r^2} = 0 \tag{16}$$

Boundary Conditions for the Fluid Phase. Since the set of partial differential two-phase flow equations (5) ,(6) ,(10) and (11) is elliptical it is necessary to define boundary conditions for all variables on all boundaries of the flow domain: inlet, exit, walls and symmetry axis.

The boundary conditions were taken the same as in single-phase flow: with universal wall functions and zero gradients at the axis and the outlet. At the inlet, mean velocity, turbulence intensity and particle volume concentration were defined.

## APPENDIX B

### Equations for Particle Motion

"Instantaneous" particle momentum equation is:

$$m^p \frac{d\vec{V}^p}{dt} = \frac{1}{2}\rho \tilde{C}_D A^p (\vec{\tilde{V}} - \vec{V}^p)|\vec{\tilde{V}} - \vec{V}^p| + \vec{\tilde{F}} \tag{17}$$

where the instantaneous drag coefficient $\tilde{C}_D$ is:

$$\tilde{C}_D = \frac{24}{\tilde{Re}^p} \tilde{f}^p \tag{18}$$

and instantaneous particle Reynolds number:

$$\tilde{Re}^p = \frac{\rho d^p |\vec{\tilde{V}} - \vec{V}^p|}{\mu} \tag{19}$$

Equation (17) is made "instantaneous" (stochastic) by generating a random fluid velocity field around the particle ($\vec{\tilde{V}}$) on the basis of known turbulence energy and time and length scales. Fluid velocity fluctuations $(u, v, w)$ are generated independently as random numbers from a Gaussian distribution with a mean of zero and a standard deviation $(u', v', w')$, which can be determined from the local value of kinetic energy of turbulence:

$$u' = v' = w' = \sqrt{\frac{2}{3}k} \tag{20}$$

The fluctuating components of fluid velocity $(u, v, w)$ are then added to the determined mean fluid velocity components $(U, V, W)$ to obtain the "instantaneous" values of fluid velocity $(\tilde{u}, \tilde{v}, \tilde{w})$ which are needed in the equation (17) for particle motion. The fluid instantaneous velocity components $(\tilde{u}, \tilde{v}, \tilde{w})$ are kept constant until the local Lagrangian integral time scale $T_L$ expires, which corresponds to the "lifetime" of large eddies. $T_L$ can be estimated from local values of kinetic energy of turbulence and it's dissipation:

$$T_L = 0.3\frac{k}{\epsilon} \tag{21}$$

The "size" of an eddy estimated from local length scale of turbulence $L_L$ is:

$$L_L = u' T_L \tag{22}$$

This model enables direct accounting for the relative motion between the eddy and the particles, hence enables determination of the effect of crossing trajectories. Particle–eddy interaction is stopped when: either the eddy lifetime is over or when particle crosses the eddy. Then a new fluctuation velocity component is generated.

Boundary Conditions for the Particles. Boundary conditions for the particles have to be defined on the inlet, on the walls and the axis. The inlet particle velocity can be given or assumed known from experiments. On the walls and the axis, a model of simple reflection is used:

$$\tilde{u}_R^p = -\psi_R \tilde{u}^p \tag{23}$$

where

$$\psi_R = \begin{cases} 0-1 & \text{on the wall} \\ 1 & \text{on the axis} \end{cases} \tag{24}$$

Table 1. Test conditions

| | |
|---|---|
| Velocity in the 42.5$mm$ pipe | 3.3$m/s$ |
| Velocity in the 21.1$mm$ pipe | 13.2$m/s$ |
| Reynolds number (42.5$mm$) | 170000 |
| Reynolds number (21.1$mm$) | 340000 |
| Average particle diameter | 430$\mu m$ |
| Particle concentration | 0 and 2% (volume) |
| Temperature | 30$^oC$ |
| Exposure time | up to 48$h$ |
| $NaCl$ concentration | 3$wt\%$ |

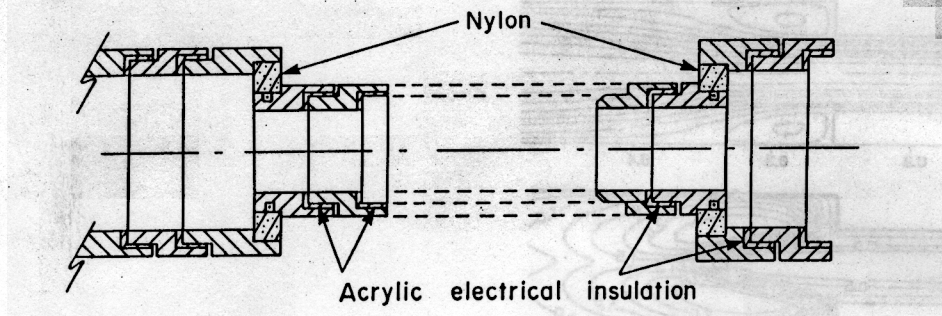


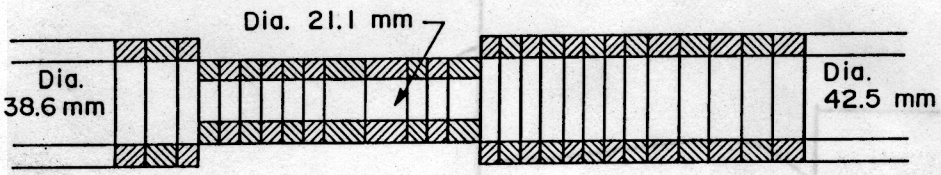


**Fig.1** Segmented test cell.

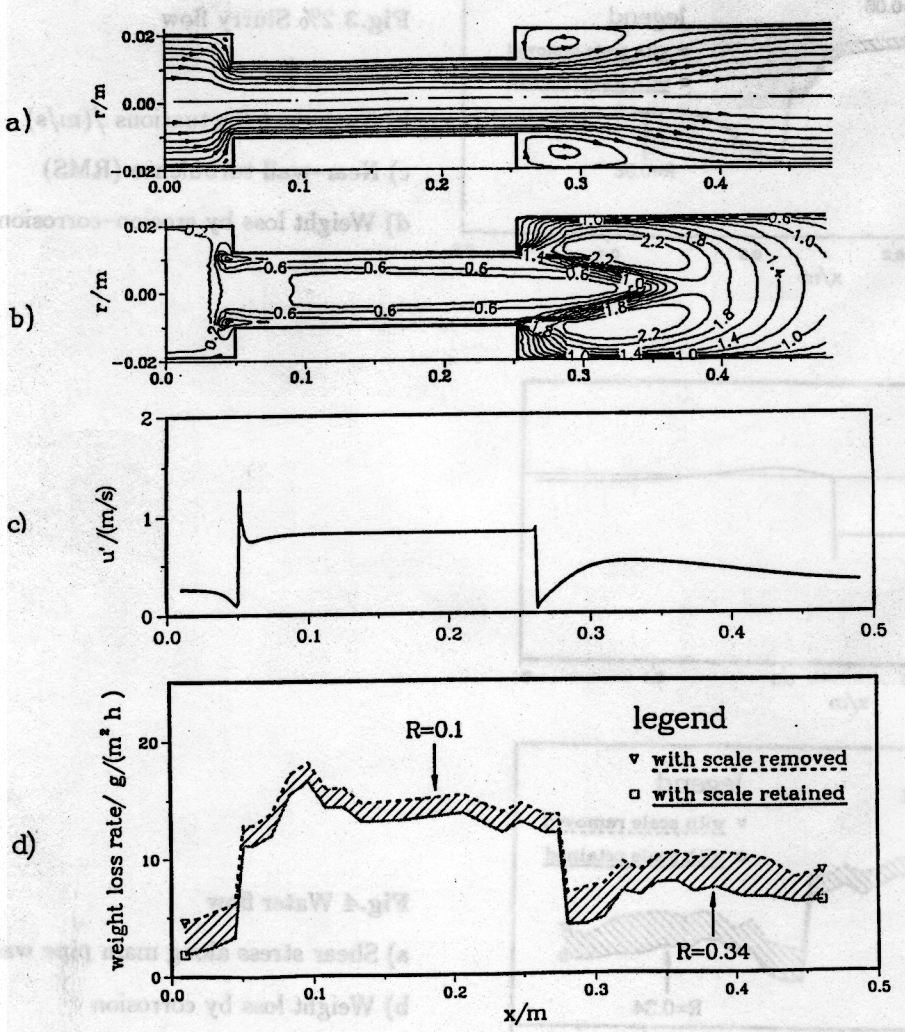


**Fig.2** Water flow

a) Streamlines

b) Turbulent fluctuations /(m/s)

c) Near-wall turbulence (RMS)

d) Weight loss by corrosion

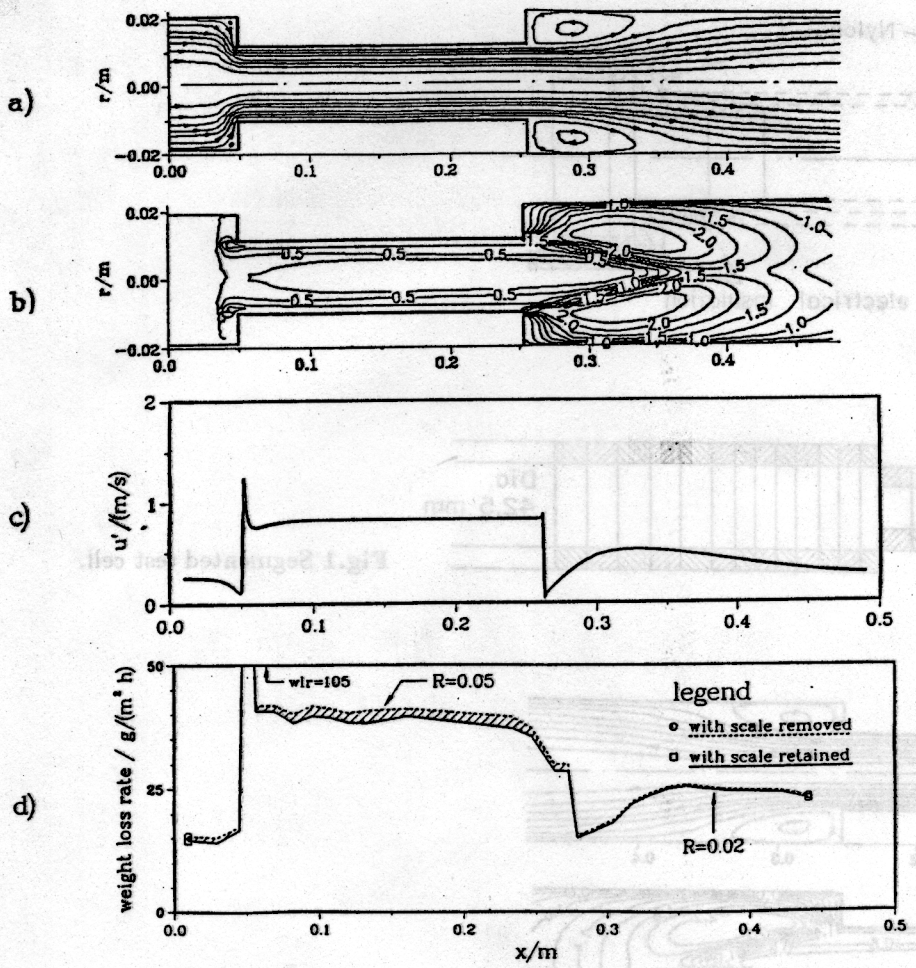


**Fig.3** 2% Slurry flow

a) Streamlines

b) Turbulent fluctuations /(m/s)

c) Near-wall turbulence (RMS)

d) Weight loss by erosion-corrosion

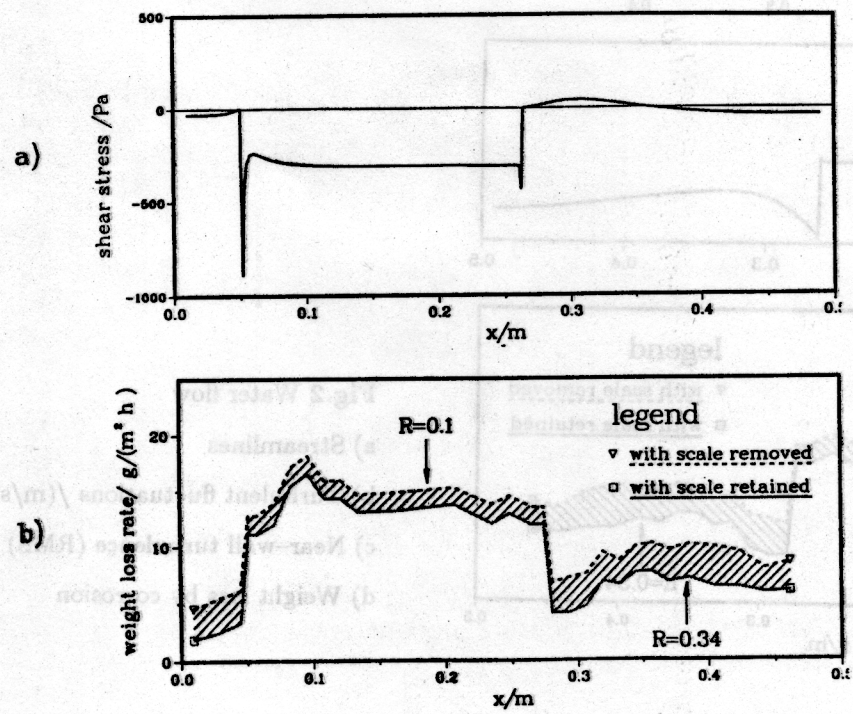


**Fig.4** Water flow

a) Shear stress along main pipe wall

b) Weight loss by corrosion